Aluminium thermal reduction process for preparing ferrosilicon and alumina from fly ash

Qixiang Su [a,b],Qingchun Yu [a,b*], Xiaomei Zhu [c*], Tianlie Xiao [a,b], Biao Ye [a,b]

[a] National Engineering Research Center of Vacuum Metallurgy, Kunming University of Science and Technology, Kunming, 650093, China
[b] Faculty of Metallurgical and Energy Engineering, Kunming University of Science and Technology, Kunming, 650093, China
[c] Faculty of Chemical Engineering, Ordos Institute of Technology, Ordos, 017000, China.
Email: 87465157@qq.com; tianlie70@163.com; 689701986@qq.com
*Corresponding author: yqcy@163.com; reozhuxm@163.com

(Received 15 July 2025; Accepted 25 March 2026)

Abstract: There has been a focus on environmental protection and the recycling of solid waste resources, particularly fly ash and aluminum dross. Increasing efforts have been made towards the utilization of fly ash in an efficient fashion. In this paper, a process was introduced for producing alumina-rich slag and ferrosilicon alloy simultaneously by means of aluminothermic reduction of fly ash with aluminium dross. Scanning electron microscopy (SEM) and energy dispersive spectroscopy (EDS) confirm the formation of spherical ferrosilicon alloy encased in a loose and porous alumina matrix during the aluminothermic reduction process. Thermodynamic calculations showed indicated that reduction temperature of SiO_2 and mullite decreased in the presence of Fe_2O_3. Under conditions of a temperature of 1673 K, ratio of aluminium dross to fly ash (A/F), and reduction time of 20 minutes, the magnetic fraction contains 85.89% ferrosilicon, while the non-magnetic fraction exhibits an alumina content of 79.42%. This process provides a solution with potential environmental and economic benefits for the application of fly ash and aluminum ash.

Keywords: Fly ash, Aluminum dross, Aluminum thermal reduction, Ferrosilicon alloy

1. Introduction

By 2024 fly ash production in China is approximately 925 million tons. About 70% of fly ash is utilized for applications on paving, filling, and soil improvement[1-4].

Nevertheless, approximately 30% of the remaining fly ash is either discarded or stockpiled due to insufficient management practices. The hazardous heavy metals will be leached when fly ash is long piled up and soaked in alkaline water. Dry ash is easy to raise dust and pollute air at windy weather, especially to the residents living in the outlet of disposal site. On the other hand, fly ash is an important secondary resource which consists of plenty of Al_2O_3, SiO_2, FeO, Fe_2O_3, and CaO [5]. Under such a circumstance, the generation of fly ash remains significant and thus its economic and green utilization technology of fly ash are desired [6].

Fly ash presents a promising opportunity for the production of alumina, alloys, and other high-value-added products. To date, a lot of methods have been proposed on the extraction of alumina from fly ash including [7] acidic methods, alkali sintering methods, acid-alkali methods, electrochemical reduction methods, etc. The typical methods for extracting Al_2O_3 from fly ash are soda-lime sintering and acid leaching. The sintering method is the most established technology for alumina extraction from fly ash, having been studied extensively [8]. This process enables a complete decomposition of mullite in fly ash, thereby facilitating the easy separation of alumina and silica [9]. Studies employing limestone sintering have demonstrated efficient alumina extraction, while also generating substantial volumes of silica slag [8,10]. To improve utility, it would be advantageous to convert silica in fly ash into high-value products during the alumina extraction process. In contrast, the acid leaching method effectively reduces waste residue and operates at lower reaction temperatures with a simplified process [11,12]. Despite these advancements, challenges remain particularly regarding low alumina extraction efficiency and the stringent requirements for acid-resistant equipment in industrial production [13]. To address these issues, pressurized leaching and microwave activation techniques have been employed to enhance extraction efficiency [14], but specialized equipment is required [15]. Both the sintering and acid leaching methods face significant hurdles in terms of industrialization due to the high silica content in fly ash [16], which leads to the production of substantial silica-containing slag. If the silica could be extracted as high-value products with recycled aluminum simultaneously, economic and environmental benefits for the process would

increase.

Besides these two typical methods, many more methods have been investigated to improve extraction efficiency. Xu proposed a novel method for extracting Al_2O_3 from fly ash by NH_4HSO_4 roasting technology [17], which includes roasting process, aluminum precipitation, alkali dissolution, carbonation decomposition and calcination. In the alumina extraction process of high-alumina fly ash, alkali could be used to remove amorphous silica and then recovered through causticization. Focusing on the causticization process, the coupling control of CO_3^{2-} conversion and $CaCO_3$ crystallization is important to secondary-pollution reduction and high-value utilization [18]. Pre-desilication is a key procedure during the elevation of Al/Si weight ratio. However, traditional desilication cannot satisfy this demand because of its low desilication ratio and the presence of abundant impurities.

Recent efforts have aimed at converting the silica in fly ash into silicon alloys. For instance, Yu et al. [19] explored the preparation of aluminum-silicon alloys through a carbothermal reduction process using fly ash at a high reduction temperature of 2473 K. Similarly, they [20] employed a comparable method to produce Al-Si-Fe alloys, which also necessitated a reduction temperature of 2373 K. Yu et al. [21-23] proposed a cost-effective approach for fabricating silicon-iron alloys and vacuum carbothermic reduction for alumina enrichment, utilizing iron oxide or CaO as an additive, which significantly lowered the reduction temperature while facilitating silica utilization. The simultaneous extraction of alumina during silicon-iron alloy production could greatly enhance the feasibility of industrial alumina recovery from fly ash. Furthermore, the resulting ferrosilicon alloy serves as an effective deoxidizer in steelmaking without harming the environment. The reduction process currently takes several hours, highlighting the pressing need to develop more economical and efficient methods to further reduce costs. They [24] soon found that the aggregation of Fe–Si alloy particles was enhanced efficiently in the presence of Na_2SO_4 during vacuum carbothermic reduction of coal fly ash. Besides, Al-Si alloy can be obtained by molten salt electrolysis of aluminum-silicon oxide extracted from coal fly ash [25]. Fu [24] thought there are the formation and decomposition of SiC and Al_4C_3. The carbothermic

reduction process of fly ash is in stages. The existence of Fe reduces the starting temperature of the Al-Si alloy formation, and helps destroy the carbide in the process of carbothermic reduction of fly ash.

Aluminum dross is a hazardous waste produced in aluminum smelting process, especially in the fields of electrolysis of alumina, casting and regeneration of aluminum[26]. Aluminum dross poses challenges in disposal and treatment. Currently, its use in construction and pavement fails to maximize its value. Aluminum dross contains valuable components like metallic aluminum and alumina. Aluminothermic reduction offers advantages over carbothermic reduction including lower reaction temperatures, and reduced carbon emission. Additionally, aluminothermic reduction of fly ash occurred at atmospheric pressure, and no caustic substance was added. This paper presents a combined process of aluminothermic reduction and magnetic separation. Aluminum dross serves as the reducing agent, and iron oxide is added as an additive. The product is separated by magnetic separation to produce magnetic ferrosilicon alloy and nonmagnetic alumina-rich slag. To optimize the aluminothermic reduction reaction, we explored various experimental parameters, including reaction temperature, reaction time, and dosage ratios. The optimal conditions ensures efficient and environmentally utilization of these solid wastes.

2 Experimental

2.1. Materials

Fly ash is from a coal-burning company in Gongyi, Henan Province, China. The chemical composition of fly ash changes over a wide range and depends on many factors like type of combusted fuel (coal, lignite, biomass), particle size of combusted fuel, temperature, and time of combustion and construction of the hearth. The main chemical components of fly ash shown in Table 1 are SiO_2, Al_2O_3, Fe_2O_3, CaO, and unburnt carbon. Additionally, the secondary components are present in fly ash in the form of MgO, Na_2O, K_2O, TiO_2. Iron oxide is analytical pure reagent. The XRD pattern (Figure 1) reveals that the predominant crystallized mineral phases are mullite ($Al_6Si_2O_{13}$) and quartz (SiO_2). A notable peak in the diffraction pattern between 20° and

30°suggests the presence of vitreous materials within the amorphous phase of the fly ash.

Table 1. *Chemical composition of fly ash*

Composition	Al_2O_3	SiO_2	Fe_2O_3	TiO_2	CaO	MgO	K_2O	Na_2O	C	Other
Content(wt%)	26.40	51.14	4.95	1.06	3.35	0.86	2.39	0.65	5.60	3.60

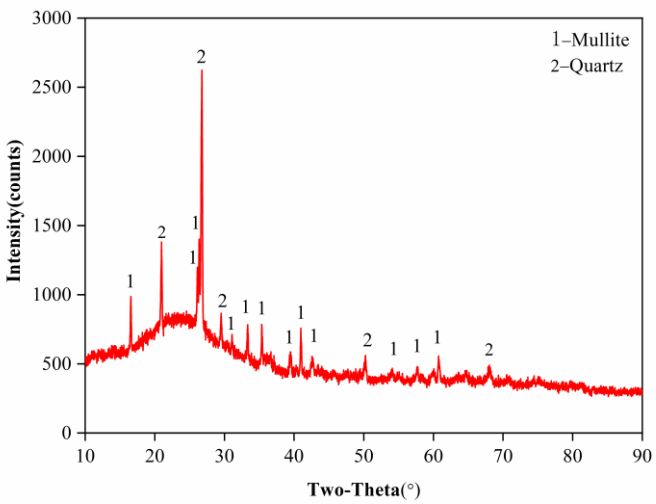

Figure 1. *XRD pattern of fly ash*

Aluminum dross is from an aluminum smelter in Gongyi, Henan Province, China. It was pretreated by drying at 378 K for 4 hours to remove moisture. No salt removal process was applied as the initial salt content was low. The material was then ground and sieved to obtain particles below 150 μm for homogeneity. XRD analysis (Figure 2.) of aluminum dross reveals a complex phase composition, including Al, Al_2O_3, aluminum nitride (AlN), magnesium aluminum spinel ($MgAl_2O_4$), SiO_2,Si, sodium iron oxide ($NaFeO_2$), and additional components. Compositions are shown in Table 2. Aluminum dross predominantly exists as metallic aluminum, alumina, aluminum nitride, and magnesium aluminum spinel. The significant presence of metallic aluminum makes its potential as an effective aluminothermic reducing agent.

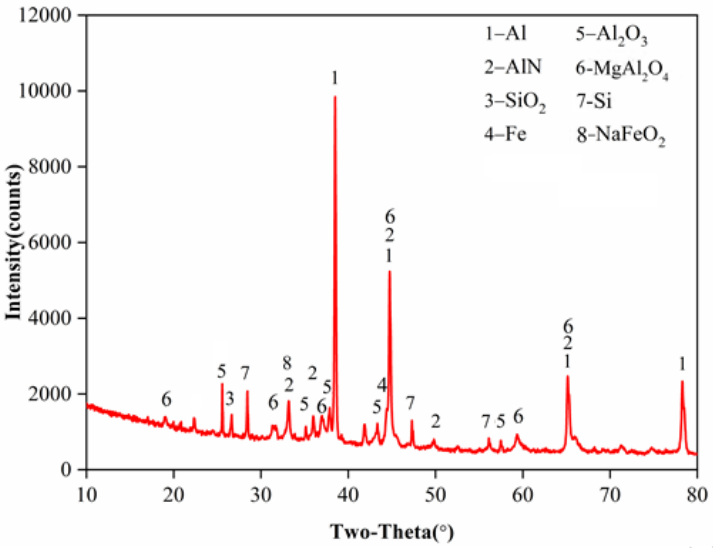

Figure 2. *XRD pattern of aluminium dross*

Table 2. *Chemical composition of aluminum dross*

Composition	Al	Al_2O_3	AlN	$MgAl_2O_4$	SiO_2	Si	Fe	$NaFeO_2$	Other
Content(wt%)	46.55	13.59	11.44	8.05	3.57	4.48	2.48	1.21	8.63

2.2. Experimental setup and procedures

Fly ash, along with aluminum dross, was grounded and mixed to achieve homogeneity. The resultant mixture was compressed into cylindrical pellets (Φ10×20 mm) under a pressure of 6 MPa and subsequently dried in an electrothermal drier to remove moisture. The obtained bulk materials was sintered in a $MoSi_2$ chamber furnace (BR-18HM-2, Bona Therm) under argon. Alumina crucibles were used. The heating rate was 10 K min^{-1}. A B-type thermocouple placed adjacent to the sample crucible was used for control and measurement. The furnace has a constant temperature volume zone of 120×120×130 mm with a uniformity of ±3 K. The holding time begins after the setting temperature. Ater the experiment, the products were ground and subjected to magnetic separation using a magnetic separator tube with a magnetizing current of 0.6 A to obtain magnetic ferrosilicon alloy and non-magnetic alumina-rich slag. The experimental schematic is illustrated in Figure 3.

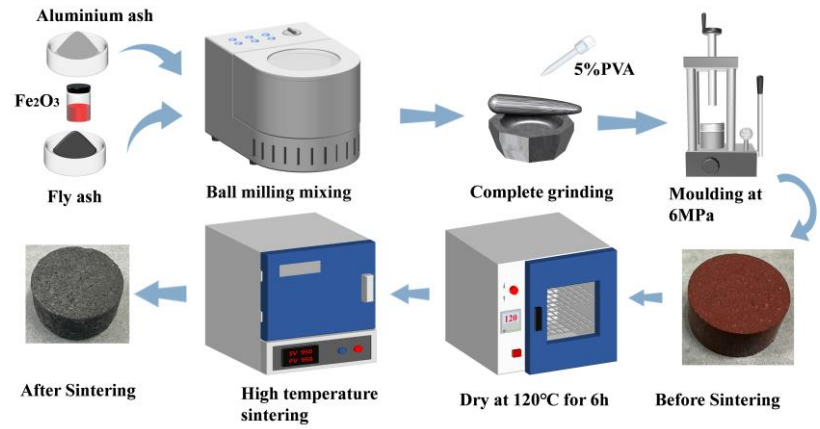

Figure 3. *Schematic diagram of the mixing and sintering process*

2.3. Characterization and analysis

The inorganic oxide content was determined using an X-ray fluorescence spectrometer (XRF, RIGAKU ZSX Primus) and chemical analysis. Scanning electron microscopy with an energy dispersive spectrometer (SEM-EDS: TESCAN, MIRA) was used to examine microstructure and elemental composition of the reduced products. X-ray diffraction (XRD, RIGAKU, SMARTLAB SE) were used to investigate the crystalline phases and composition of the samples. AlN was determined using oxygen-nitrogen-hydrogen analyzer (LECO ONH-836, LECO, USA). $MgAl_2O_4$ content was determined according to MgO content measured by EDTA complexometric titration method [27]. Al_2O_3 and total Al contents were measured by fluoride salt displacement EDTA complexometric titration method [27]. Calculation of the mass fraction of metallic aluminum was based on the volume of hydrogen gas obtained from the reaction between aluminum metal and sodium hydroxide [28]. Individual Al_2O_3 was calculated by subtracting Al_2O_3 in $MgAl_2O_4$, Al in AN, and metallic Al from the total Al content. Inductively coupled plasma optical emission spectrometer (ICP-OES) technique was adopted to measure element content of the magnetific portion. On the basis of reactions (1), (3), and (5), the theoretical ratio of aluminum dross to fly ash ratio (A/F) 0.8228:1 was obtained and labled as 1.0. Experimental conditions were optimized to maximum the conten of ferrosilicon and alumina in magnetic portion and nonmagnetic one.

3. Thermodynamics analysis

Physical and chemical properties of fly ash can be simulated as a mixture of independent components [29]. Although liquid and solid solutions may form at elevated temperatures, they have negligible effects on the final equilibrium components [30,31]. Existence state of SiO_2 is not considered. The valuable components in aluminum dross are metallic aluminum and aluminum nitride, which are used as reducing agent. There is small amount carbon in fly ash. In view of the fact that the temperature required for carbothermic reduction is significantly more than that for aluminothermic reduction, carbon in fly ash is not considered a reducing agent. According to Table 1 and 2, possible components in fly ash and aluminium dross to be reduced are Fe_2O_3, $NaFeO_2$, SiO_2, CaO, and MgO. Meanwhile, some reduction products may continue to react. The thermodynamic data were calculated using the HSC Chemistry 6.0 software package. Chemical reactions and the relationship between Gibbs free energy and temperature at standard state were summarized in Table 3.

Table 3. *Possible reactions between fly ash and aluminium dross*

Component	Number	Reaction equations	ΔG° (kJmol^{-1})
	(1)	$1/2Fe_2O_3 + Al = Fe + 1/2Al_2O_3$	-434.309+0.036T
Fe_2O_3,	(2)	$1/2Fe_2O_3 + AlN = Fe + 1/2Al_2O_3 + 1/2N_2(g)$	-111.002-0.078T
$NaFeO_2$	(3)	$NaFeO_2 + Al = Fe + 1/2Al_2O_3 + 1/2Na_2O$	-339.345+0.014T
	(4)	$NaFeO_2$+AlN= $1/2Fe+1/2Al_2O_3+1/2Na_2O+1/2N_2(g)$	-16.040-0.100T
	(5)	$3/4SiO_2 + Al = 3/4Si + 1/2Al_2O_3$	-159.053+0.029T
	(6)	$3/8Al_6Si_2O_{13}+Al=13/8Al_2O_3+1/2Si$	-168.756+0.042T
	(7)	1/3SiO2+5/18Fe2O3+Al=1/9Fe5Si3+1/2Al2O3	-341.216+0.034T
	(8)	$3Al_6Si_2O_{13}$+5Fe2O3+18Al=2Fe5Si3+18Al2O3	-345.529+0.039T
	(9)	Si+C=SiC	-77.553+0.015T
	(10)	Fe+Si=FeSi	-80.746+0.006T
SiC,	(11)	$Fe+2Si=FeSi_2$	-97.998+0.033T
Si,	(12)	$Fe+1/3Si=1/3Fe_3Si$	-36.911-0.005T
Fe	(13)	$Fe+3/5Si=1/5Fe_5Si_3$	-52.639+0.002T
	(14)	$2/9SiC+1/9SiO_2+Fe=1/3Fe_3Si+2/9CO(g)$	55.899-0.037T
	(15)	$2/5SiC+SiO_2+Fe=1/5Fe_5Si_3+2/5CO(g)$	114.419-0.074T

Iron oxide exists in the form of Fe_2O_3 and $NaFeO_2$. SiO_2 exists as quartz, mullite, and amorphous glass in fly ash. Possible aluminothermic reduction reactions are the reactions (1)- (8). The relationship between standard Gibbs free energy change (ΔG°)

and temperature is illustrated in Figure 4(a). With increasing temperature, the standard Gibbs free energy variation of reactions (2) and (4) shows a decreasing trend, while an opposite tendency is found for that of reactions (1), (3), and (5)-(8). However, ΔG° for these reactions are much less than zero. It is evident that these reactions are thermodynamically favorable ($\Delta G^\circ < 0$) within the investigated temperature range.

The aluminothermic reduction reaction of mullite and quartz phase can occur at experimental temperatures as shown in Figure 4 (a). However, it is interesting to find that when there is Fe_2O_3 in the reduction system, the standard Gibbs free energy variation of aluminothermic reduction mullite and quartz reduces 200 $kJmol^{-1}$. Consequently, the existence of Fe_2O_3 can efficiently reduce the aluminothermic reduction temperature of mullite and quartz from the thermodynamics perspective.

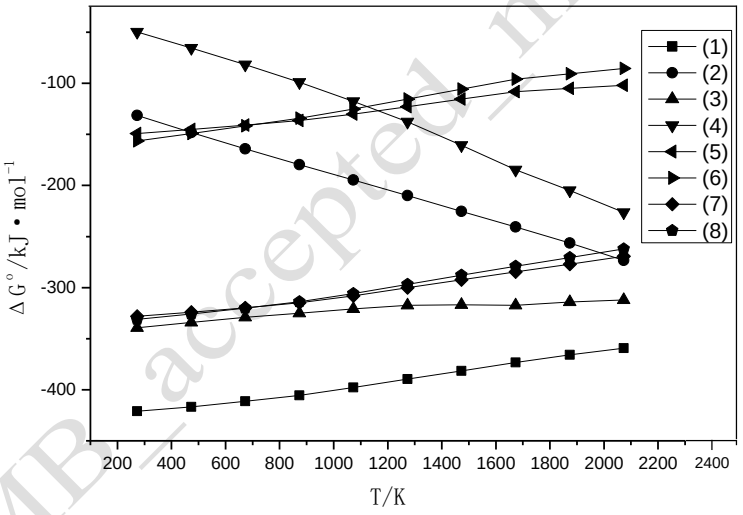

(a)

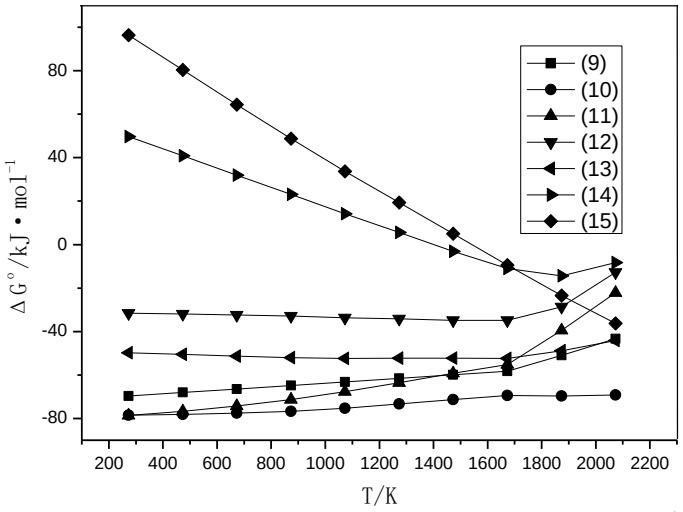

(b)

Figure 4. Diagrams of the ΔG° -T for possible reactions: (a) reactions (1)-(8); (b) reactions (9)-(15)

Aluminothermic reduction reaction products may interact among themselves or with some components in fly ash and aluminium ash continuously. As shown in Fig 4 (b), there is a significant decrease in the standard Gibbs free energy variation of the reactions (14) and (15) with increasing temperature, and the initial reaction temperature can be obtained as 1408.163K and 1560.264K, respectively. A slight increase in standard Gibbs free energy variation of reactions (9) – (11) is found except a slight decrease for the reactions (12) and (13). It is noted that there are distinct inflection points for reactions (9), and (11) – (14), implying a decrease of possibility of reactions occurrence after inflection points. However, standard Gibbs free energy variation of reactions are below zero in the temperature range of 1546.2-2073.15K, which means these reactions may occur spontaneously.

On the whole, thermodynamic analysis shows that standard Gibbs free energy variation of aluminothermic reduction of Fe_2O_3, $NaFeO_2$, and SiO_2 with aluminum nitride is much higher than that of metallic aluminum (Figure 4 (a)), which means that metallic aluminum serves as an effective reducing agent at a lower temperature than aluminum nitride. CaO and MgO can't be reduced by aluminum or aluminum nitride. Iron reduced

in the presence of iron oxide more easily combines with silicon to form a trace liquid phase, which further reduces the activity of Si and promotes the reaction to the right. In addition, the Gibbs free energy changes of reactions (10) – (13) prove that when the generated Si and Fe exist, reaction products such as $FeSi_2$, Fe_3Si and Fe_5Si_3 can be produced at experimental temperatures.

4. Results and discussion

4.1 Effect of temperature

Experiment of aluminothermic reduction of fly ash using aluminum ash in the temperature range of 1473 K - 2073 K was made. The X-ray diffraction (XRD) patterns of the reduction products were shown in Figure 5.

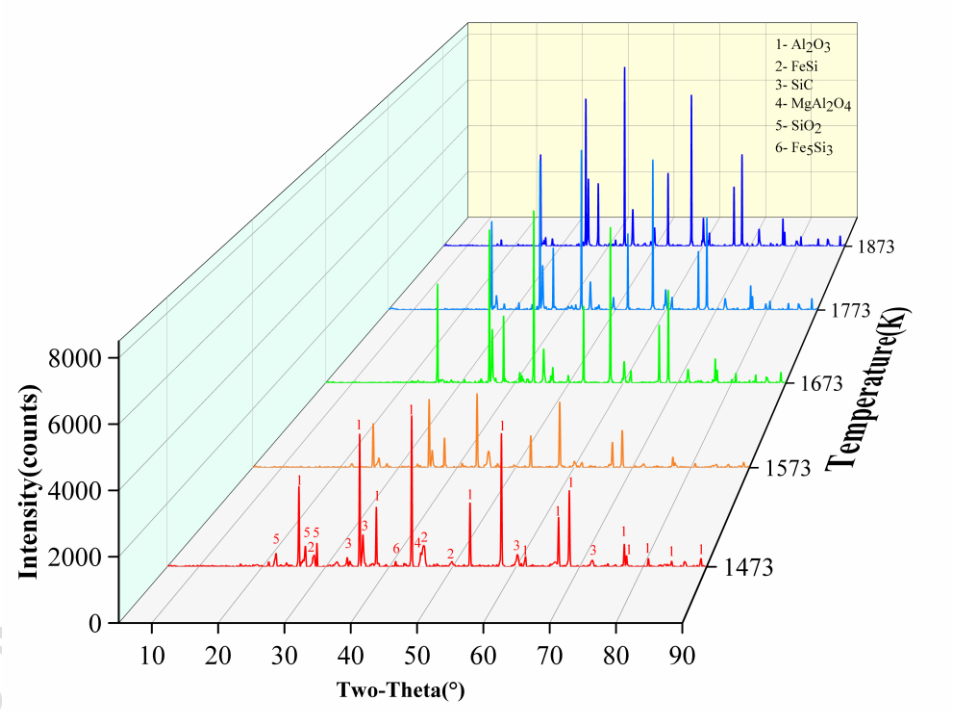

Figure 5. *XRD patterns of reduction products in range of 1473-1873K*

It is observed that the primary component in the reaction products is Al_2O_3, along with FeSi, SiC, $MgAl_2O_4$, SiO_2, and Fe_5Si_3. No mullite was found, indicating that mullite has been completely decomposed. The decomposition of mullite is favorable for the separation and extraction of silica and alumina. At 1473 K, SiO_2 is present in the product. However, as the temperature increases, the characteristic peak intensity of SiO_2

becomes weaken due to the reduction by aluminum according to Eq(5). This observation promotes the production of ferrosilicon alloy. The intensities of the characteristic peaks for SiC increases with increasing temperature, meaning that Si obtained reacts with the residual carbon in fly ash by reaction (9). Meanwhile, a lot of iron and silicon are obtained and reacts to produce Fe_5Si_3 by reaction (13), which is in agreement with the increase of diffraction intensity of Fe_5Si_3. $MgAl_2O_4$ spinel was also found in the product because the reaction between MgO and Al_2O_3 can occur at relatively low temperature [32].

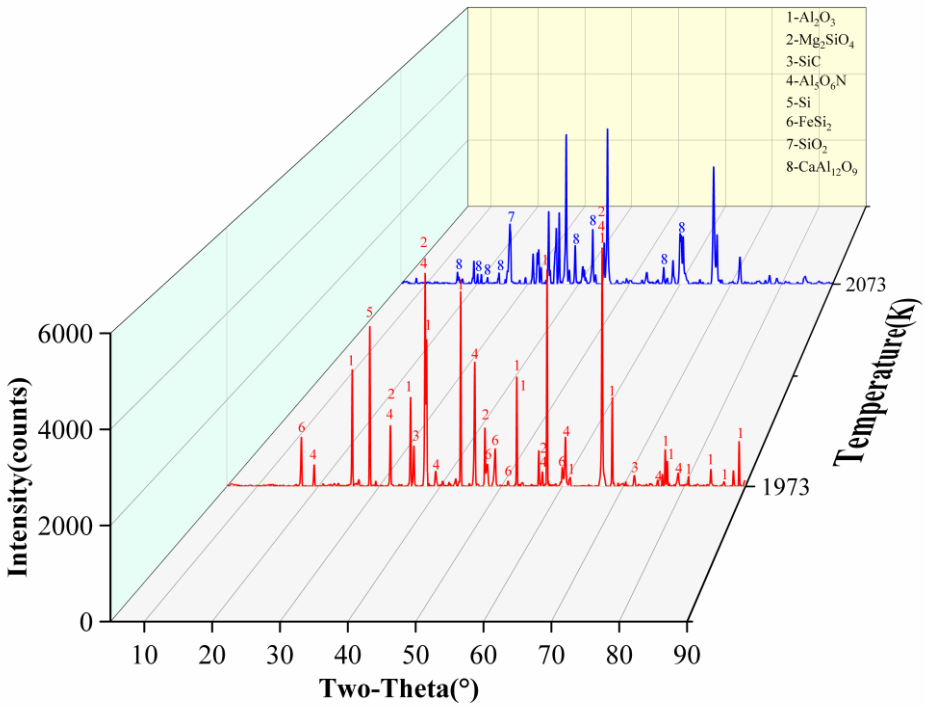

(a) upper slag

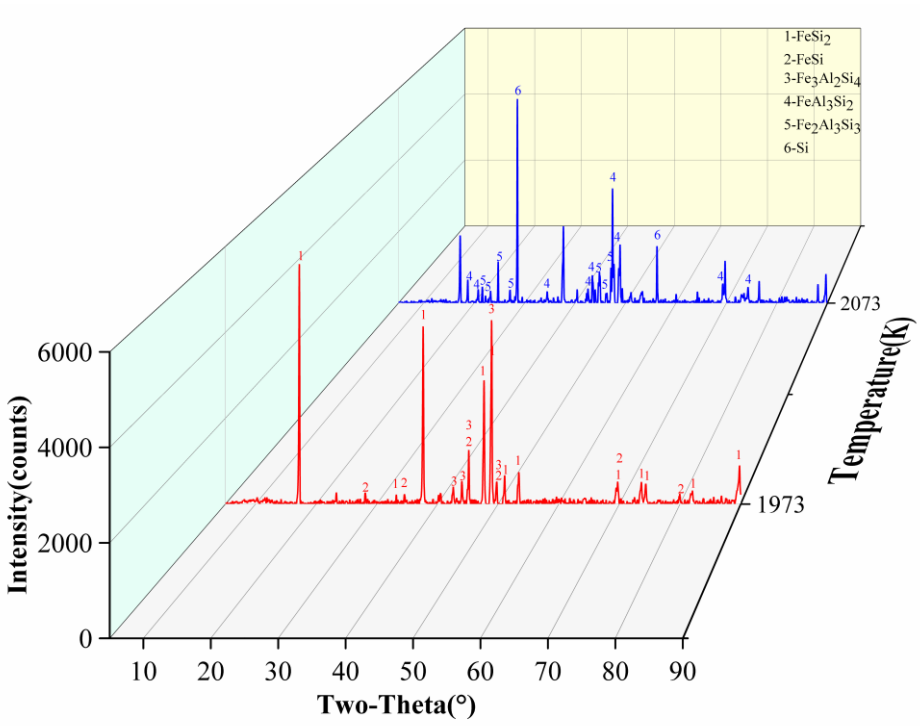

(b) Bottom alloy

Figure 6. *XRD patterns of the reduction products in range of 1973-2073K*

The melting point of ferrosilicon is generally between 1683K and 1733K. When the temperature exceeds 1773K, ferrosilicon alloy becomes liquid at high temperatures. Fluidity of the molten slag is poor. During the process of aluminum thermal reduction of fly ash, reactions (2) and (4) will also occur. Under the action of N_2 gas, it will separate from the alloy phase. When the temperature is more than 1873K, notable changes in the products are observed. The product develops a distinct layered structure, namely slag layer and metal layer, which provides convenience for the separation of ferrosilicon from slag. Figure 6(a) and (b) present the X-ray diffraction (XRD) patterns of the upper slag and bottom alloy in the temperature range of 1973K-2073K, respectively. As shown in Figure 6(a), the detection of Mg_2SiO_4 signifies the occurrence of a reaction between MgO and SiO_2. $MgAl_2O_4$ was absent from the slag layer. MgO preferentially reacts with Al_2O_3 to form $MgAl_2O_4$ with a volume expansion, following by a volume shrinkage due to the production of Mg_2SiO_4. Additionally, the presence of an Al_5O_6N diffraction peak and the concurrent decrease in Al_2O_3 intensity imply that AlN reacts with Al_2O_3 to form Al_5O_6N [33]. Correspondingly, presence of Al_5O_6N will lead to the loss of Al_2O_3 in alumina-rich slag. Various diffraction peaks of ferrosilicon

alloy including $FeSi_2$ and FeSi at 1973 K are found in Figure 6(b), which is probably caused by a higher production of silicon by reaction (5). This observation means $FeSi_2$ and FeSi, not Fe_3Si and Fe_5Si_3, are major products at higher temperature. Appearance of Al-Si-Fe alloy at 2073K means the decrease of aluminum content in the slag phase, which is against the recovery of alumina-rich slag. Taking these factors into consideration, it is recommended that the optimal holding temperature this process is 1673 K.

4.2 Effect of time

Effect of time on the reduction of fly ash was examined in a range of 5 - 30 minutes, with a temperature of 1673 K and theoretical addition of aluminum ash. Figure 7 presents the X-ray diffraction (XRD) patterns of the reduction products.

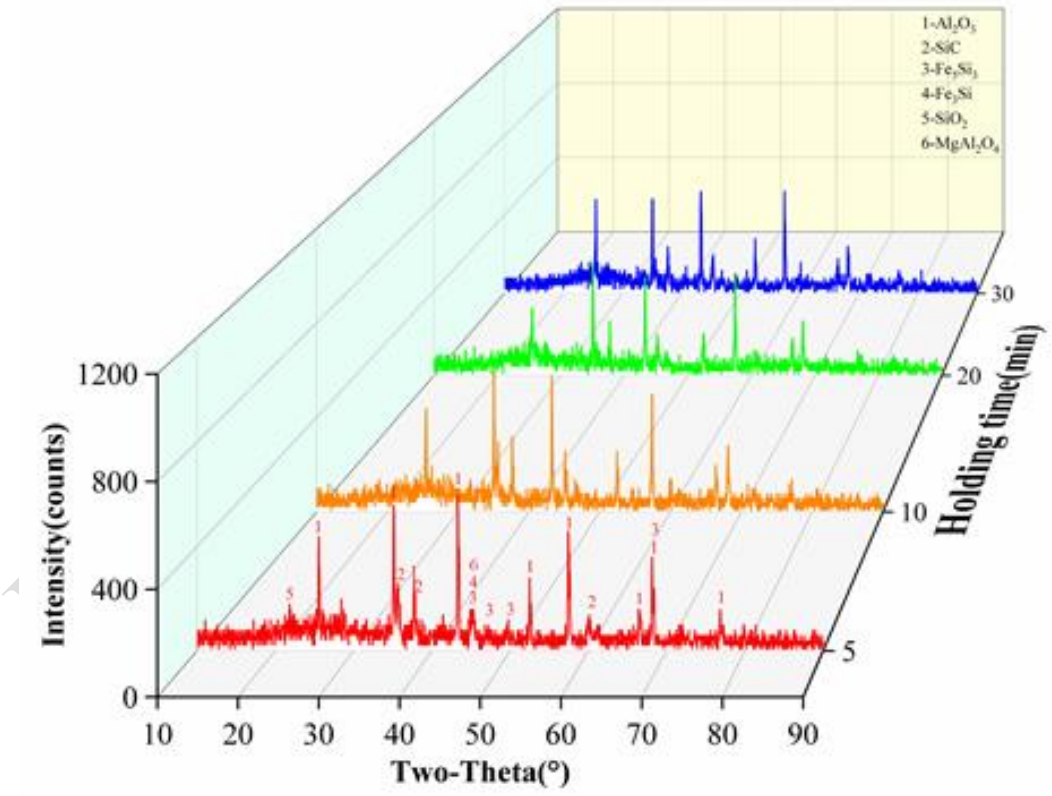

Figure 7. *XRD patterns of reduction products in different times*

The diffraction peaks remain nearly identical across different reaction times. The phases identified include Al_2O_3, FeSi, SiC, $MgAl_2O_4$, Fe_5Si_3, and SiO_2, but the intensity of diffraction peaks varies throughout the time range. The diffraction peak of mullite in

fly ash disappears in 5 minutes, indicating that the decomposition of mullite into SiO_2 and Al_2O_3 occurs. The XRD patterns show that the SiO_2 phase remains detectable in 5 - 10 minutes, but the intensity of its diffraction peaks gradually decrease due to the reaction (5). By the time 20 minutes, the characteristic peak of SiO_2 disappears and is replaced by spinel phase. SiC is formed in the initial stage of aluminothermic reduction process and subsequently reacts with silicon dioxide and iron to produce a ferrosilicon alloy by reactions (14) and (15). Similarly, intensity of the characteristic peak for SiC declines over time. However, SiC cannot be fully consumed due to the insufficient Fe. In light of the reduction of SiO_2 and SiC, the optimal holding time is proposed to be 20 minutes.

4.3 Effect of aluminium dross

On the basis of reactions (1), (3), and (5), the theoretical ratio of aluminum dross to coal fly ash ratio (A/F) was obtained and labled as 1.0. Effect of aluminium dross addition with different ratios of aluminum dross to fly ash (A/F) at a temperature of 1673K and in 20minutes was investigated. XRD analysis of the reduction products is shown in Figure 8.

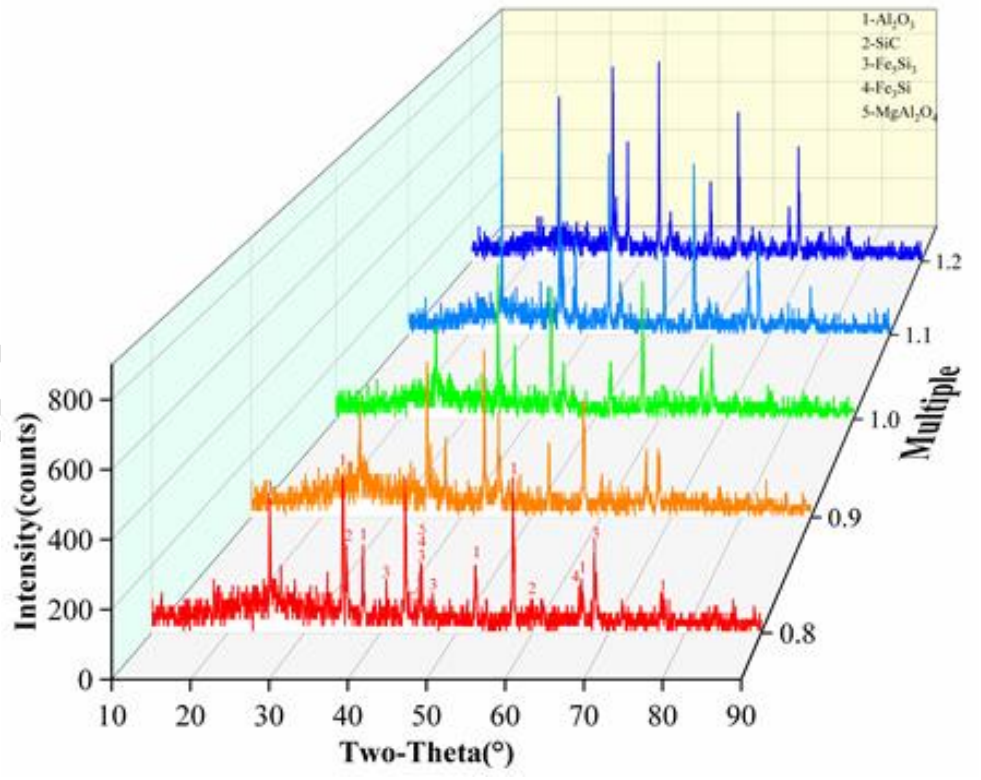

Figure 8. *XRD patterns of reduction reaction products with different ratios of raw materials*

It is evident that the phases of the reaction products remain consistent within the ratio range of 0.8 - 1.2. The primary phases identified are Al_2O_3, FeSi, SiC, $MgAl_2O_4$, and Fe_5Si_3. Neither mullite nor SiO_2 is present indicating a complete decomposition of mullite and deep involvement of SiO_2 during the aluminothermic reduction process. Consequencely, diffraction peaks intensity of silicon-containing phases such as SiC, Fe_5Si_3 and Fe_3Si increase. The characteristic peak intensity of SiC initially decreases and then increases with the lowest peak strength at a ratio of 1.0. Taking into account the participation of SiO_2 in the reaction and the corresponding response of SiC, the optimal A/F value is established at 1.0.

4.4 Separation of ferrosilion alloy and alumina-rich salg

Aluminothermic reduction of fly ash experiment was made under optimal conditions. The reaction products obtained were grounded and subjected to magnetic separation to obtain the magnetic and non-magnetic materials shown in Figure 9(a) and (b). Magnetic portion is dark black, and the nonmagnetic one is lighter than the former.

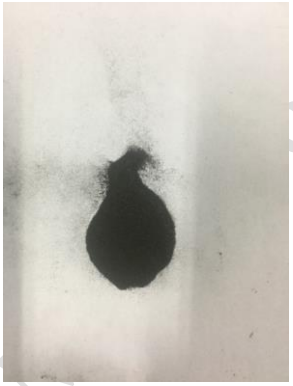

(a) magnetic materials

(b) nonmagnetic materials

Figure 9. *Physical map of product : (a) magnetic materials; (b) nonmagnetic materials*

XRD patterns of magnetic and non-magnetic materials are presented in Figure 10. There is still some Al_2O_3 in the the magnetific materials due to the incomplete separation. Consequently, a small amount ferrosilicon alloy such as Fe_5Si_3 and Fe_3Si stays in the non-magnetific materials shown in Fig 10.

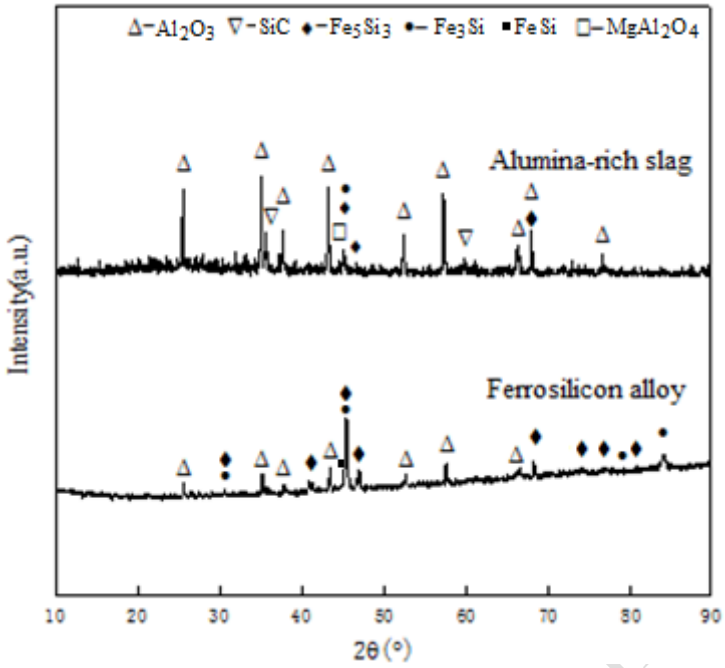

Figure 10. *XRD patterns of product: (a)Magnetic materials; (b)Nonmagnetic meterials*

Chemical composition of the magnetic portion was presented in Table 4. The ferrosilicon alloy contained 63.84 wt% Fe, 22.05 wt% Si, 7.28% Al, and 3.24 wt% C. A Fe/Si of 2.9 indicats that reduction amount of iron oxide is more than that of alumina. Alumina content in nonmagnetic portion is 79.42% by chemical analysis. Alumina-rich slag with a alumina content of 10% is obtained, which can be used as a raw material for extracting alumina. Solid wastes are transformed into valuable substances. Accordingly, amount of fly ash and aluminum dross will be reduced greatly when aluminum, silicon and iron are fully extracted.

Table 4. Chemical composition of magnetic portion

Element	Fe	Si	Al	C
Mass (wt%)	63.84	22.05	7.28	3.24

4.5 Morphology of reduction products

Products were analyzed using scanning electron microscopy (SEM) and energy dispersive spectroscopy (EDS). Figure 11(a) shows the morphology of the sample after

grinding. In Figure 11(a), spherical particles are evident, accompaning by irregularly-shaped materials. Figure 11(b) presents a magnified view of the area indicated in Figure 11(a). Figure 11(c) shows the cross-sectional morphology of the sample, which reveal the circular white areas alongside the irregularly-shaped gray regions. The black areas in the samples represent pores formed during the reaction; these voids are attributed to the formation and escape of gases throughout the aluminothermic reduction process. A spherical Fe–Si particle embedded in a porous alumina matrix is found in Figure 11(d). Point and surface scanning using energy dispersive spectroscopy (EDS) is shown in Figure 12. Figures 12(a) and 12(b) correspond to points 1 and 2 in Figure 11(d), respectively. The elemental composition at point 1 is O 6.04 wt.%, Al 2.71 wt.%, Si 26.79 wt.%, and Fe 64.47 wt.%, indicating that the white circular area is mainly composed of a ferrosilicon alloy. The elemental composition at point 2 is O 47.04 wt.%, Al 48.70 wt.%, Si 2.71 wt.%, and Fe 1.55 wt.%, suggesting that the irregular material is characterized as loose and porous alumina. Due to the incomplete separation, small amount of alumina and ferrosilicon alloy stays in the magnetic materials and nonmagnetic materials, respectively.

Si and Fe are concentrated in the white circular regions in Figures 12(d) - (g), whereas O and Al are found in the gray irregular regions and along the periphery of the circular areas in Figure 11 (c), such as pink portion. This distribution indicates that Al and Si originally combined in mullite, are influenced by Fe. During aluminothermic reduction process, these elements are spatially separated at a microscopic level, leading to the reduction of iron and silicon and the formation of liquid phase micro-regions within a specific compositional range. These liquid phase areas ultimately converge in the voids of the sample, resulting in the growth of ferrosilicon alloy particles.Furthermore, the decomposition of mullite yields alumina, which remains in solid form due to its high melting point. Consequently, solid alumina is retained in its original position, manifesting as loose, porous, and irregularly shaped particles. This structural characteristic is essential for facilitating the subsequent physical separation of ferrosilicon alloy and alumina-rich slag. By grinding and magnetic separation, ferrosilicon alloy and alumina-rich slag can be obtained. Meanwhile, there are a lot of

tiny spherical ferrosilicon alloy particles shown in figure 12(c). Small amount of ferrosilicon alloy is found in the alumina-rich slag due to the incomplete separation.

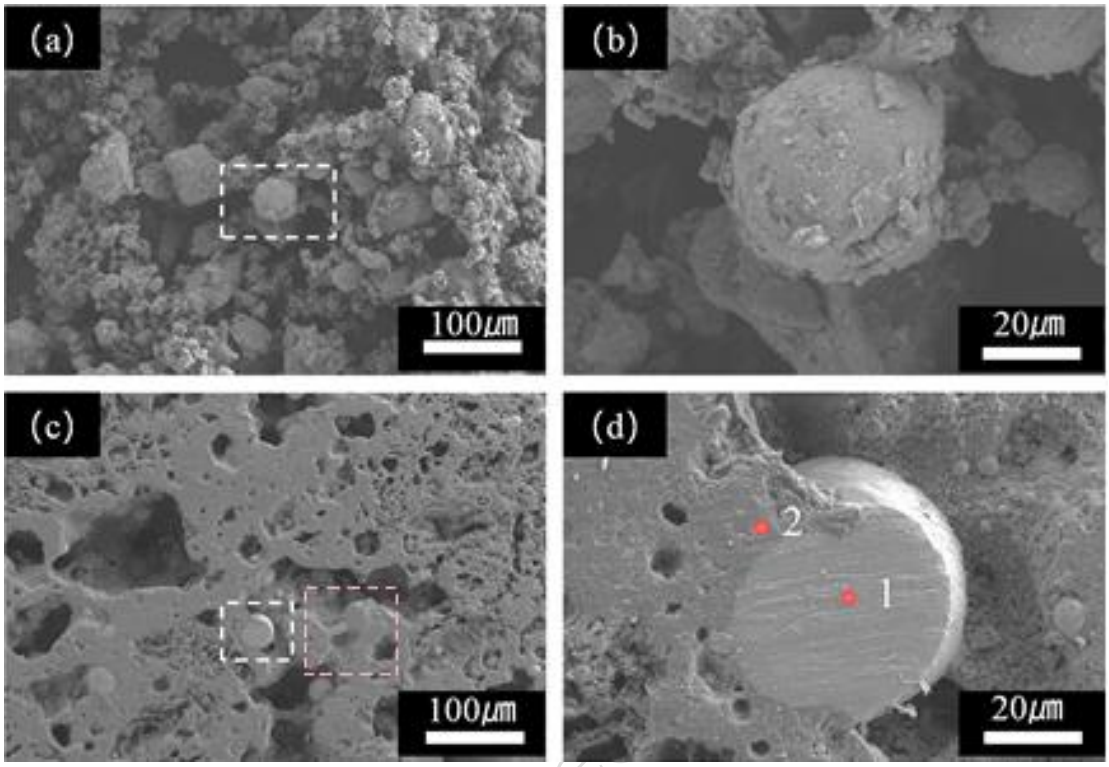

Figure 11. *SEM images of sample powder: (a) morphology; (b) morphology of the selected area; (c)cross-section morphology; (d) cross-section morphology of the selected area*

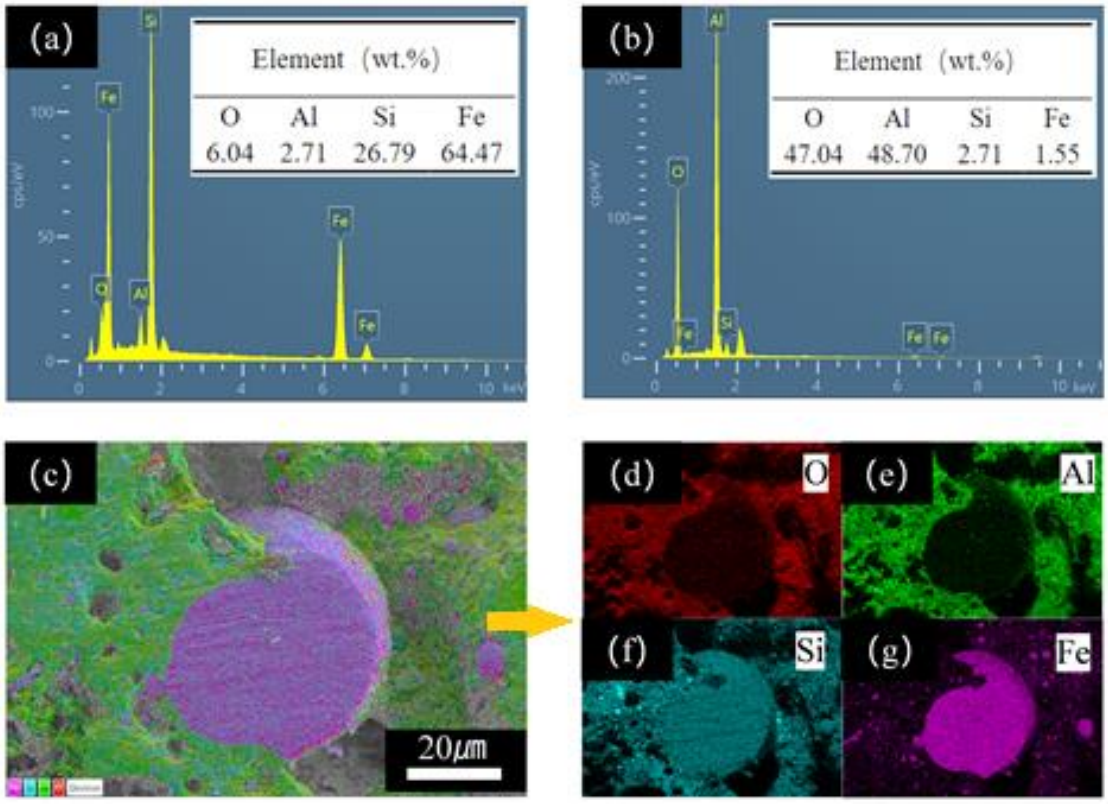

Figure 12. *EDS patterns: (a, b) EDS spectra at points 1 and 2 in Figure 11(d); (c) composite elemental map; (d–g) elemental distribution maps for O, Al, Si, and Fe, respectively*

The process mainly composed of two stages. The first stage is the formation of ferrosilicon alloys during the aluminothermic reduction. And the second one is the separation of alumina and ferrosilicon alloys by sieving and magnetic separation. Fly ash and aluminum dross are both waste to be handled. The process delivered appropriate conditions for the subsequent utilization in dustry. The residual amount of waste is greatly shortened when ferrosilicon alloy and alumina are extracted from fly ash and aluminum dross. It is suggested that the aluminothermic reduction and magnetic sepatation may provide an environmentally friendly means for large-scale utilization of fly ash and aluminum dross.

5 Conclusions

This study successfully demonstrates a sustainable metallurgical process for the recovery of ferrosilicon alloy and alumina-rich slag from fly ash and aluminum dross through aluminothermic reduction and magnetic separation. The main findings can be summarized as follows:

(1) Aluminum dross proves to be an effective reducing agent. With the addition of Fe_2O_3, the theoretical reduction temperatures of mullite and quartz are greatly reduced. Phases of FeSi and Fe_5Si_3 are found 1473K. Ferrosilicon including $FeSi_2$ and FeSi is found at 1973 K. Al-Si-Fe alloy appears at elevated temperature such as 2073K. SiC is formed in the initial stage of aluminothermic reduction process and subsequently reacts with silicon dioxide to produce ferrosilicon.

(2) At 1673K and A/F ratio of 1.0, when the reaction time is 20 minite, ferrosilicon and alumina content both are optimal, yielding a ferrosilicon content of 85.89% (Fe_3Si and Fe_5Si_3) in magnetic portion and an alumina content of 79.42% in nonmagnetic one. Small amount of aluminum and carbon is left in the magnetic portion due to incomplete separation.

(3) Ferrosilicon alloy can be used in steelmaking, and alumina-rich slag can be used a

raw material to extract alumina. Meanwhile, when silicon, aluminum, and iron are extracted from fly ash and aluminum dross, residual amount of these waste reduced greatly. The prosess offers a solution with potential environmental and economic benefits for the application of industrial waste.

Acknowledgments
Funding: This work was supported by the National Natural Science Foundation of China [grant No.52364054].

Authors contributions
Investigation, Biao Ye; conceptualization, Xiaomei Zhu; methodology, Tianlie Xiao; writing—review and editing, Qixiang Su and Tianlie Xiao; supervision, Qingchun Yu. All authors have read and agreed to the published version of the manuscript.

Data availability
The raw data supporting the conclusions of this article will be made available by the authors on request.

Conflict of interest
The authors declare no conflict of interest.

References

[1] Z. Li, Y. Ji, H. Ma, P. Zhao, X. Zeng, S. Liu, Y. Jiang, L. Wang, A. Liu, H. Gao, F. Liu, J. K. Mwangi, Characterization of inorganic elements within PM2.5 and PM10 fractions of fly ashes from coal-fired power plants, Aerosol and Air Quality Research, 17(4)(2017)1105-1116. https://doi.org/10.4209/aaqr.2017.02.0071

[2] Z. Yao, X. Ji, P. K. Sarker, J. Tang, L. Ge, M. Xia, Y. Xia, A comprehensive review on the applications of coal fly ash, Earth-Science Reviews, 141(2015)105-121. https://doi.org/10.1016/j.earscirev.2014.11.016

[3] T. Hemalatha, A. Ramaswamy. A review on fly ash characteristics e Towards promoting high volume utilization in developing sustainable concrete, Journal of Cleaner Production, 147 (2017) 546-559. http://doi.org/10.1016/j.jclepro.2017.01.114

[4] L. Li, H. Yu, H. Ma, C. Wu, N. Zhang, N. Wang, Theoretical foundation, hydration mechanism, and concrete performance of basic magnesium sulfate, Journal of Building Engineering, 111 (2025) 113120. https://doi.org/10.1016/j.jobe.2025.113120

[5] Y. Guo, Y. Li, F. Cheng, M. Wang, X. Wang, Role of additives in improved thermal activation of coal fly ash for alumina extraction, Fuel processing technology, 110(2013) 114-121.

https://doi.org/10.1016/j.fuproc.2012.12.003

[6] X. Zhuang, L. Chen, S. Komarneni, C. Zhou, D. Tong, H. Yang, W. Yu, H. Wang, Fly ash-based geopolymer: clean production, properties and Applications, Journal of Cleaner Production, 125(2016) 253-267. https://doi.org/10.1016/j.jclepro.2016.03.019

[7] A. Liu, Z. Shi, K. Xie, X. Hu, B. Gao, M. Korenko, Z. Wang. Extraction of Al–Si Master alloy and alumina from coal fly ash, Journal of Mining and Metallurgy, Section B: Metallurgy. 2017, 53 (2) B : 155 – 162. https://doi.org/10.2298/JMMB160616006L

[8] C. Liu, S. Zheng, S. Ma, Y. Luo, J. Ding, X. Wang, Y. Zhang, A novel process to enrich alumina and prepare silica nanoparticles from high-alumina fly ash, Fuel processing technology, 173(2018) 40-47. https://doi.org/10.1016/j.fuproc.2018.01.007

[9] Z. Jiang, H. Ma, J. Yang, X. Ma, J. Yuan, Thermal decomposition mechanism of desilication coal fly ash by low-lime sinter method for alumina extraction, Ferroelectrics, 486(1) (2015) 143-155. https://doi.org/10.1080/00150193.2015.1100878

[10] Z. T. Yao, M. S. Xia, P. K. Sarker, T. Chen. A review of the alumina recovery from coal fly ash, with a focus in China, Fuel, 120(2014) 74-85. https://doi.org/10.1016/j.fuel.2013.12.003

[11] L. Yan, J. Shang, Y. Wang, J. Li, H. Liu, T. Qu, C. Zhang. Experimental parameter optimization study on the acid leaching of coal fly ash, Desalination and Water Treatment, 57(23) (2016) 10894-10904. https://doi.org/10.1080/19443994.2015.1040463

[12] A. K. Tripathy, B. Behera, V. Aishvarya, A. R. Sheik, B. Dash, C. K. Sarangi, B. C. Tripathy, K. Sanjay, I.N. Bhattacharya. Sodium fluoride assisted acid leaching of coal fly ash for the extraction of alumina, Minerals Engineering, 131(2019) 140-145. https://doi.org/10.1016/j.mineng.2018.10.019

[13] N. Nayak, C. R. Panda, Aluminium extraction and leaching characteristics of Talcher Thermal Power Station fly ash with sulphuric acid, Fuel, 89(1) (2010) 53-58. https://doi.org/10.1016/j.fuel.2009.07.019

[14] A. Shemi, R.N. Mpana, S. Ndlovu, L.D. van Dyk, V. Sibanda, L. Seepe. Alternative techniques for extracting alumina from coal fly ash, Minerals Engineering, 34(2012) 30-37. https://doi.org/10.1016/j.mineng.2012.04.007

[15] P. Wang, H. Liu, F. Zheng, Y. Liu, G. Kuang, R. Deng, H. Li, Extraction of aluminum from

coal fly ash using pressurized sulfuric acid leaching with emphasis on optimization and mechanism, JOM, 73(9) (2021) 2643-2651. https://doi.org/10.1007/s11837-021-04801-z

[16] Z. Zhang, X. Qiao, J. Yu, Aluminum release from microwave-assisted reaction of coal fly ash with calcium carbonate, Fuel Processing Technology, 2015, 134: 303-309. https://doi.org/10.1016/j.fuproc.2014.12.050

[17] D. Xu, H. Li, W. Bao, C. Wang, A new process of extracting alumina from high-alumina coal fly ash in NH_4HSO_4+H_2SO_4 mixed solution, Hydrometallurgy, 165 (2016) 336–344. https://doi.org/10.1016/j.hydromet.2015.12.010

[18] G. Zhu, H. Li, R. Lin, S. Li, X. Hou, Q. Tang, Synthesis of superfine calcium carbonate during causticization in highly alkaline system for utilization of high-alumina fly ash, Hydrometallurgy, 165(2016) 282-289. https://doi.org/10.1016/j.hydromet.2016.01.022

[19] Q. Yu, Y. Deng, Y. Feng, Z. Li, Phase Transformation of Alumina, Silica and Iron Oxide during Carbothermic Reduction of Fly Ash, Metals, 11(8) (2021) 1165. https://doi.org/10.3390/met11081165

[20] Q. Yu, Y. Deng, S. Yin, Z. Li. Thermal process for magnesium production with Al-Si-Fe from coal fly ash: thermodynamics and experimental investigation, Journal of Mining and Metallurgy, Section B: Metallurgy, 57(3) (2021) 421-430. https://doi.org/10.2298/JMMB210118038Y

[21] H. Chen, W. Yu, Z. Jiang, W. Jiang, P. Wei, J. E. Nyarko-Appiah. Fe-Si alloys production and alumina extraction from coal fly ash via the vacuum thermal reduction and alkaline leaching. Fuel Processing Technology 244 (2023) 107702. https://doi.org/10.1016/j.fuproc.2023.107702

[22] W. Yu, Z. Rao, H. Yuan, P. Wei, J. E. Nyarko-Appiah a,b, Weiyan Jiang. An efficient and environmental friendly strategy for alumina extraction and Fe–Si alloys production from coal fly ash by combining vacuum thermal reduction, alkali dissolving, and magnetic separation. Journal of Cleaner Production 408 (2023) 137129. https://doi.org/10.1016/j.jclepro.2023.137129

[23] H. Yuan, W. Yu, J. Wen, F. Yang, J. E. Nyarko-Appiah, C. Bai. A new strategy for CO_2 storage and Al_2O_3 recovery from blast furnace slag and coal fly ash by employing vacuum reduction and alkali dissolution methods. Energy. 308(2024)

132865. https://doi.org/10.1016/j.energy.2024.132865

[24] J. E. Nyarko-Appiah, W. Yu, L. Song, P. Wei, H. Chen. The Enhancing mechanism of Na_2SO_4 on mullite decomposition and alumina recovery during the vacuum carbothermic reduction of coal fly ash. Journal of Sustainable Metallurgy. 10(2024): 810-821. https://doi.org/10.1007/s40831-024-00832-3

[25] Z. Liu, M. Guo, H. Niu, C. Wang, C. Fan, B. Gao. A novel process for producing Al-Si alloy utilizing aluminum-silicon oxide extracted from coal fly ash. Process Safety and Environmental Protection 191 (2024) 390–400. https://doi.org/10.1016/j.psep.2024.08.065

[26] X. Wu, Q. Zhao, X. Yu, Q. Shen, Y. Lin. Environmental protection treatment and resource utilization of aluminum dross. Metallurgical and Materials Transactions B. 56(2025): 4218-4229. https://doi.org/10.1007/s11663-025-03622-8

[27] Chemical analysis of magnesia-alumina refractories. National Standards of the People's Republic of China (GB/T 5069-2024) https://www.doc88.com/p-39216336782942.html

[28] Methods for chemical analysis of aluminum dross. Henan nonferrous metals industry association group standard. https://www.doc88.com/p-61473463292470.html

[29] J. Tomeczek, H. Palugniok, Kinetics of mineral matter transformation during coal combustion, Fuel, 81(2002) 1251–1258. https://doi.org/10.1016/S0016-2361(02)00027-3

[30] Q. Qiu, V. Hlavacek, S. Prochazka, Carbonitridation of Fly Ash. I. Synthesis of SiAlON-Based Materials, Industrial & Engineering Chemistry Research, 44(2005) 2469–2476. https://doi.org /10.1021/ie0497036

[31] C. A. Pickles, Thermodynamic analysis of the selective carbothermic reduction of electric arc furnace dust, Journal of Hazardous Materials, 150(2008) 265–278. https://doi.org/10.1016/j.jhazmat.2007.04.097

[32] J. Liu，C. Zhang, Research status of low-temperature synthesis and sintering of $MgAl_2O_4$ spinel, Nonferrous Metals Design, 45(2) (2018) 104-110. no DOI (*in Chinese*)

[33] X. Tan, Z. Zhao, P. Chen, X. Li, B. Zhu, Effect of nano metallic Fe on Al_5O_6N Synthesis in Al_2O_3-C refractories, InterCeram: International Ceramic Review, 64(2015) 108–111. https://doi.org/10.1007/bf03401110

List of figures

List of tables